JOURNAL OF MATERIALS SCIENCE 28 (1993) 1031–1036

Patterns of stress-induced phase transformation in MgO-stabilized zirconia ceramic revealed using micro-Raman imaging

M. BOWDEN, G. D. DICKSON, D. J. GARDINER*
Department of Chemical and Life Sciences, University of Northumbria, Ellison Place, Newcastle upon Tyne NE1 8ST, UK

D. J. WOOD
Directorate General of Defense Quality Assurance, Royal Arsenal East, Woolwich, London SE18 6TD, UK

An automated Raman microscope system has been used to collect mapped Raman data from a Goodfellow 3% MgO stabilized zirconia ceramic tile. The data have been transformed to produce images which show the relative concentrations and distributions of the monoclinic and tetragonal phases in the mapped areas. The images reveal concentrations of the monoclinic phase at grain boundaries. Regions surrounding indents in the tile created with a Vickers hardness tester, were also mapped to reveal the extent and pattern of stress-induced phase transformation. A Raman map was also generated from an area before and after indentation. Comparison of the Raman images with the optical white light images reveals a relationship between the pattern of grain boundaries on the sample and the distribution of transformed material.

1. Introduction

Zirconia, ZrO_2, exists in three phases [1] with a monoclinic structure below 1100 °C. Above this temperature it transforms over a 100 °C range to a tetragonal structure which is stable to 2370 °C, whereupon it transforms to a cubic structure which is stable until it reaches its melting point at 2770 °C. The high melting point of zirconia suggests that it has a great potential for high-temperature applications. Most metallic components, by comparison, lose strength at around 1100 °C. Two major problems that prevent zirconia being used as high-temperature components are its brittleness compared to metals and the volume difference, of approximately 9%, associated with the tetragonal to monoclinic transformation. The latter would prevent any form of temperature cycling because the components would fracture.

It has long been known, however, that by adding rare-earth oxides such as MgO, Y_2O_3 or CaO, it is possible to stabilize ZrO_2 in the tetragonal phase at room temperature, thus creating a material of great mechanical strength which retains its properties over a large temperature range.

There has been considerable interest in zirconia as an engineering ceramic ever since it was first shown that transformation toughening could be used to enhance the fracture toughness of the material. Transformation toughening occurs when the stabilized tetragonal material transforms to the monoclinic phase under applied stress; this can considerably strengthen the material. For example, if a crack is created in the ceramic, the stress field ahead of the crack tip will create a transformed zone; as the monoclinic phase has a larger volume than the tetragonal phase, the transformation can act to seal the crack and so prevent catastrophic failure.

The unit cell of monoclinic ZrO_2 has four zirconium atoms with each zirconium atom surrounded by seven oxygen atoms [2, 3]. The oxygen atoms are arranged in two, nearly parallel planes, forming a square on one side and a triangle on the other. When zirconia transforms to the tetragonal phase [4] the coordination of the zirconium atoms changes from seven to eight. This change has been shown by X-ray diffraction (XRD) studies to occur by a rotation of the triangularly arranged oxygen atoms and a small shift of the oxygen atoms in the square arrangements [5]. This diffusionless shear mechanism, where all the atoms retain their nearest neighbours, is typical of a martensitic transformation. Other experimental evidence also confirms the martensitic character of the monoclinic to tetragonal transformation [6, 7].

There have been many Raman studies reported on the ZrO_2 system, including low spatial resolution

* Author to whom all correspondence should be addressed.

0022–2461

profiling [8] and a 30 μm scale map of the phase transformations around a diamond indent [9, 10]. Studies of phase transformation due to fracture have also been reported [11, 12], including a study using an imaging photomultiplier tube [13]. Kudo *et al.* [14] have used an automated stepper motor-driven Raman microscope in conjunction with an intensified multichannel detector to generate Raman maps. These maps were represented with concentric circles having diameters related to species concentration. It has already been demonstrated [15, 16] that there are regions of high monoclinic content at grain boundaries and at areas which have been stressed with, for example, a Vickers hardness indentor. To try and gain a better understanding of the way in which the monoclinic distribution responds to the indentation and the role of the grain boundaries, a series of Vickers hardness indents were made in a Goodfellow 3% MgO-stabilized ZrO_2 ceramic tile. The loads used were: 30, 20 and 10 kg. The areas around the indents and the surrounding grain boundaries were Raman mapped at different spatial resolutions.

2. Experimental procedure

Raman mapping has been approached in several different ways and the overall approach employed here has been described in detail elsewhere [15]. The mapping and imaging system is based on a BGSC RMIII Raman microscope coupled to a Spex Triplemate employing an intensified diode array detector. The sample is moved beneath the microscope by computer-controlled stepping motors. The data are collected by the camera control computer, and are then transferred to a data analysis computer and transformed into a set of 700 Raman images of the sample, each at one particular wavelength. These images can be arithmetically manipulated before being displayed as a greyscale using up to 64 shades available on a VGA monitor. Typical instrument conditions used to collect the map data were a laser power of 10 mW, exposure time of 115 s, ×60 objective, a 200 μm spatial filter defining a ~ 3.5 μm spot on the sample, and a spectral resolution of 1 cm^{-1}.

3. Image processing

Raman spectra of the monoclinic and the tetragonal forms of ZrO_2 are shown in Fig. 1. In order to present image data which reflect the varying concentrations of the two forms of ZrO_2 it would be necessary to use the intensities of Raman bands characteristic of each form and corrected for the differing Raman scattering cross-sections. Various formulae are presented in the literature, most are modelled on analogous formulae used in XRD and are based on the relative intensities of the most distinctive bands at 181, 192 and 264 cm^{-1}. Clark and Adar [11] used the formula

$$C_m = \frac{I_{m181} + I_{m192}}{F(I_{t148} + I_{t264}) + I_{m181} + I_{m192}} \quad (1)$$

where C_m is the monoclinic concentration, I_m and I_t refer to monoclinic and tetragonal bands, respectively,

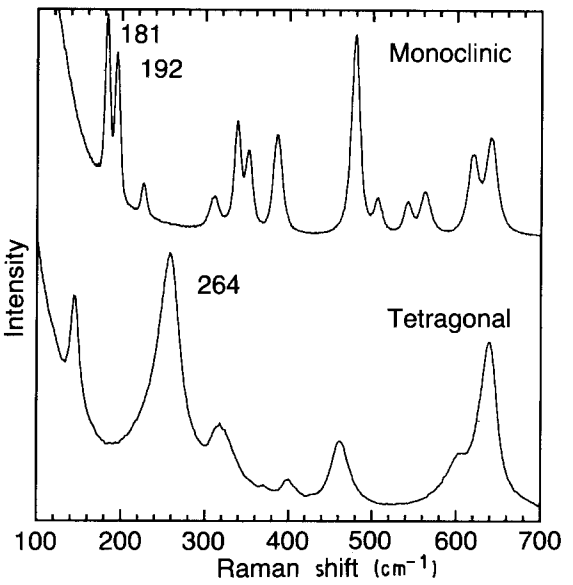

Figure 1 Raman spectra of tetragonal and monoclinic zirconia.

F is a "factor required to convert the Raman intensities to the XRD intensities of the reference material", and was determined to be 0.97. Ohtaka and Kume [17] used an identical equation in their work on the synthesis of orthorhombic zirconia but they determined that the F factor was 4.

Ishitani *et al.* [18] used a slightly altered formula

$$C_m = \frac{I_{m181} + I_{m192}}{4.4I_{t146} + I_{m181} + I_{m192}} \quad (2)$$

in which they considered only the bands at 181, 192 and 146 cm^{-1}.

These inconsistencies can be understood as the XRD equations, on which the Raman equations are modelled, and which are based on several assumptions which do not always hold [19–21]. In order to make any definite statements about the relative amounts of phases present, it would be necessary to study the spectra of samples of known composition. We have measured relative intensities for the two phases both as pure materials and as mixtures and have shown that the Raman doublet at 181, 192 cm^{-1} in the monoclinic phase is ~ 30 times stronger than the 264 cm^{-1} band in the tetragonal phase. The accuracy of this result is, however, questionable because the powders used differed in particle size. For these reasons we have not attempted to produce quantitative concentration images. The images presented here were produced by representing each image pixel by the ratio of the monoclinic 181, 192 cm^{-1} doublet to the sum of the tetragonal 264 cm^{-1} and monoclinic 181, 192 cm^{-1} bands (C_m) after background subtraction

$$C_m = \frac{I_{m181} + I_{m192}}{I_{t264} + (I_{m181} + I_{m192})} \quad (3)$$

The method by which the spectroscopic data are transformed into image data, is discussed elsewhere [15].

The contrast of the resulting images has been adjusted such that the regions of highest C_m are shown as

black, and regions where C_m is zero are shown as white with intervening grey shades.

4. Results and discussion

4.1. 30 kg indent

A photograph of the 30 kg Vickers indent is reproduced in Fig. 2. A corner of the diamond indent occurs near to the point where the three grain boundaries meet in the centre of the picture. The region shown in Fig. 2, measuring 100 μm × 75 μm, was mapped with a step interval of 5 μm. The resulting Raman image is shown in Fig. 3, where it can be seen that there are areas of high monoclinic content along the grain boundaries and within the grain in the top left-hand quadrant. Comparison of the distribution of monoclinic phase across a grain boundary in unstressed ceramic (3–6 μm, see later) with the apparent width of the monoclinic phase across the stressed grain boundaries here (10–12 μm), suggests that a measure of stress relief has occurred.

4.2. 20 kg indent

A close-up of the 20 kg indent is shown in Fig. 4. It can be seen that the indent just cuts across the vertical grain boundary in the centre-left of the picture and ends near a small microcrystallite. The 100 μm × 100 μm area was mapped using a 5 μm step interval, and the resulting Raman map is shown in Fig. 5. The Raman map shows that the left-hand side of the mapped area has been transformed to the monoclinic phase, whereas the right-hand side appears to remain largely tetragonal. The small, apparently untransformed region on the left-hand side, is an artefact resulting from the laser being out of focus at the bottom of the indent. Again the grain boundaries appear to have an important role in the transfomation process. The edge of the transformed zone coincides closely with the grain boundary which would appear to act as barrier to the transformation. There are two other areas of interest; the line of transformation which runs parallel to the top diagonal grain boundary and the circular area which appears light grey and stretches from the corner of the indent to the horizontal grain boundary at the bottom of the picture. The white light microscope image provides no obvious explanation for these features which are most probably caused by micro cracks surrounding the diamond indent. A

Figure 2 White light image of 30 kg indent region showing mapped area.

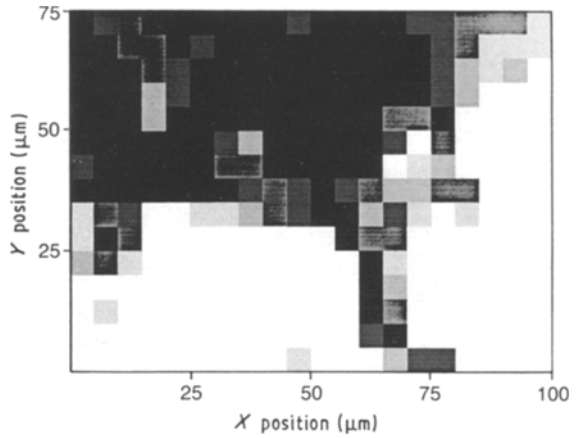

Figure 3 Raman map (100 μm × 75 μm) of 30 kg indent region.

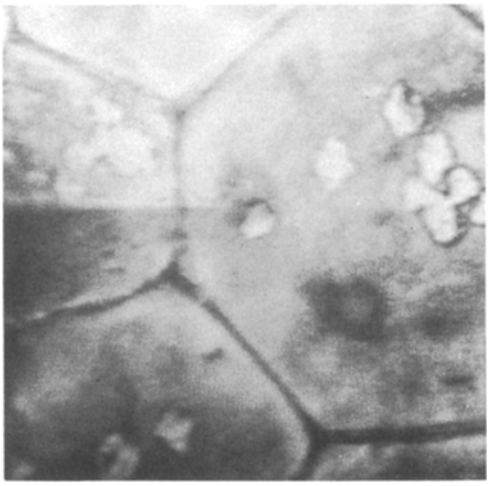

Figure 4 White light image of 20 kg indent region showing mapped area.

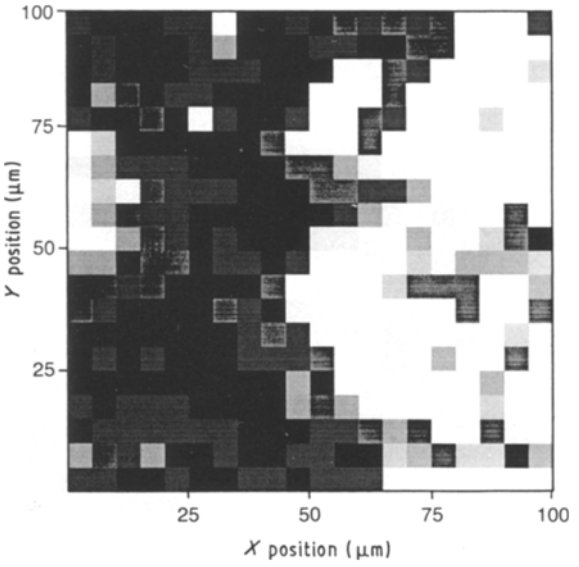

Figure 5 Raman map (100 μm × 100 μm) of the 20 kg indent region.

small crack can just be resolved under the microscope stretching from the diamond indent to the grain boundary, it seems probable, therefore, that there may be other small cracks which are not resolved.

4.3. 10 kg indent

The 10 kg diamond indent is shown in Fig. 6. The area around the right-hand corner of the indent was mapped with a 5 μm step size over a 125 μm × 100 μm region. The Raman map is shown in Fig. 7. An interesting feature revealed by the map is that transformation has occurred in a grain which is adjacent to the one in which the indent corner ends. Once again, the extent of the transformation is limited by the grain boundaries. In the grain containing the indent corner, the transformation region is very much restricted to the actual indented area, and there is also another transformed region which runs parallel to the diagonal grain boundary from the indent corner. It can be seen that the transformed region around the diamond indent ends on the microcrystallite situated just in front of the indent corner. The transformed region which runs parallel to the grain boundary, extends from the indent corner to the large circular dark feature at the bottom of the photograph. This pattern of transformation is possibly due to microcracking in the material.

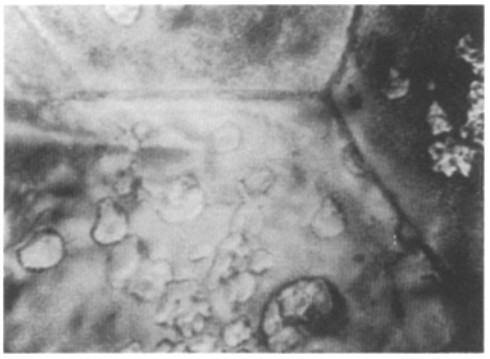

Figure 6 White light image of 10 kg indent region showing mapped area.

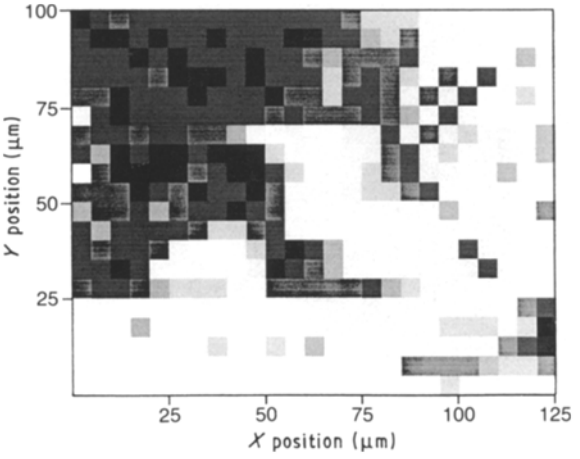

Figure 7 Raman map (125 μm × 100 μm) of 10 kg indent region.

4.4. Map of zirconia, before and after indentation

In order to confirm the role of the grain boundaries in the pattern of phase transformation, the distribution of the monoclinic phase was mapped before and after the sample was indented. To carry this out it was necessary to map an area of the sample 100 μm × 100 μm, remove the sample and then relocate the same area under the Vickers hardness indentor and place an indent in the mapped region. To accomplish this the sample was first fixed on to the XY stepping stage and an easily identifiable feature was chosen as an origin of an XY coordinate system. After recording the first set of Raman data, the sample was transferred to the Vickers hardness indentor and the coordinate system was used to position the indent. A second set of Raman data were then collected. The mapped region is shown in Fig. 8; this region was selected because it consists of four grains, which are larger than average and because there are relatively few microcrystallites and no other features which could be regarded as defects. The four large grains were mapped using a 3 μm step size over a 70 × 70 step grid.

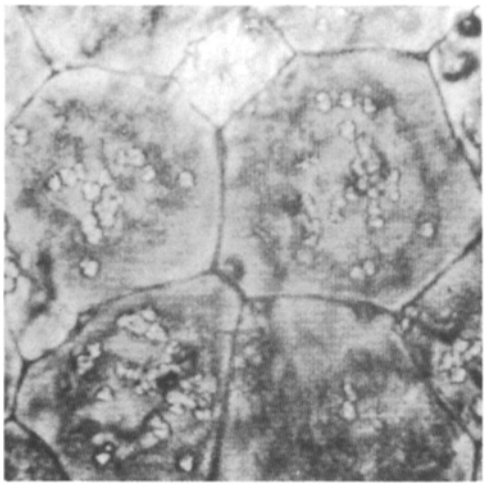

Figure 8 White light image of zirconia ceramic before indentation, showing mapped area.

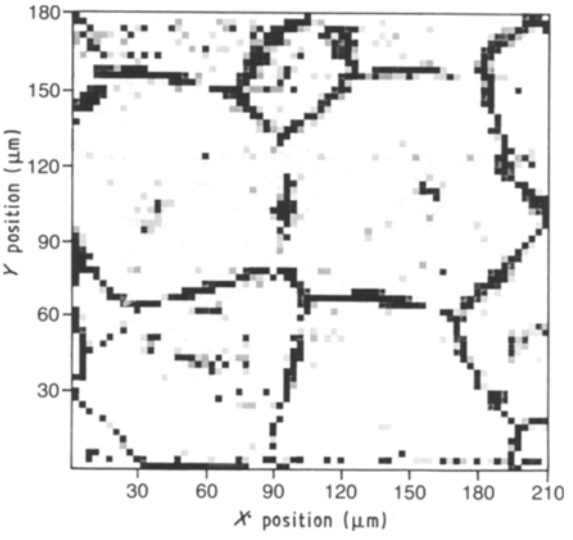

Figure 9 Raman map (210 μm × 210 μm) of zirconia ceramic before indentation.

At this time only low laser powers (< 5 mW at the sample) were available to us and, consequently, much longer integration times had to be used to obtain acceptable spectra. To collect this map the Raman system ran continuously for 70 h. As before, the data were processed by integrating over the monoclinic band, subtracting wings at each side as background, and then dividing by the integrated intensity of the tetragonal and monoclinic bands minus their approximated backgrounds. The Raman map before indentation is shown in Fig. 9. It clearly shows the same grain structure that can be seen in the white light image of Fig. 8 and demonstrates that the sample is predominantly in the tetragonal phase but with a higher content of the monoclinic phase at the grain boundaries. The map also confirms that the width of the monoclinic region across the grain boundaries is 3–6 μm and that there are no inclusions, or invisible cracks which have created transformed zones in the unstressed sample.

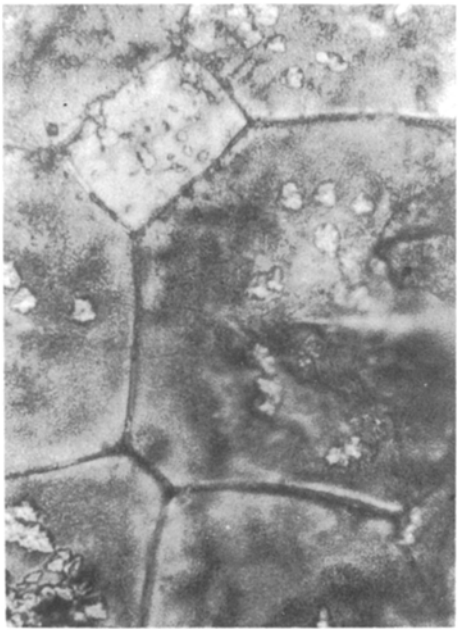

Figure 10 White light image of zirconia ceramic after indentation, showing mapped area.

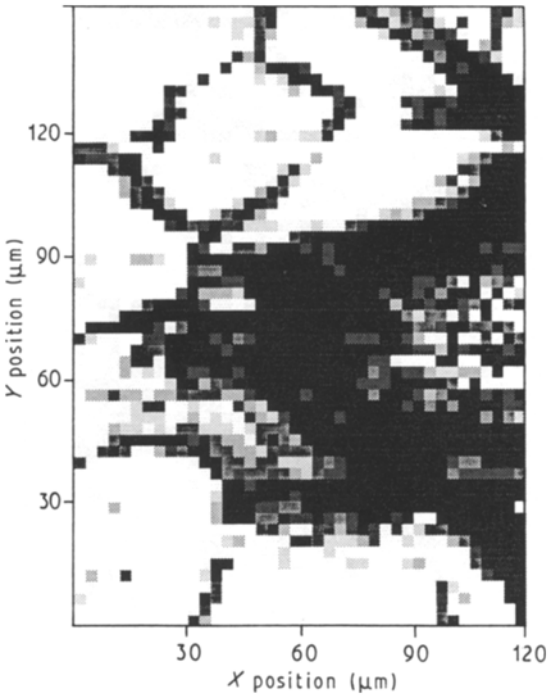

Figure 11 Raman map (120 μm × 150 μm) of zirconia ceramic after indentation.

The sample was then removed from the XY stepper stage and fixed to an XY micrometer stage. The sample positioned under the Vickers hardness indentor and an indent was made in the sample using the 10 kg load. Fig. 10 shows a smaller region of the sample after indentation where the corner of the indent is clearly visible in the right-hand grain. An area surrounding this grain was mapped and is shown in Fig. 11. Although this map is of a smaller area than the previous one, the smaller rectangular grain at the top of the picture can be used to relate the two. All the features observed in the previous indents are apparent here. The two horizontal grain boundaries both show broadening and the bottom grain boundary appears to act as a barrier to transformation. There is a transformed region running diagonally upwards from the top horizontal grain boundary which cannot be related to grain structure and could therefore be assigned to microcracking induced in the material. The transformed region from the crack corner crosses the vertical grain boundary, whereas the white light image of Fig. 10 clearly shows that the indent stops about 30 μm short of this boundary.

5. Conclusions

This work demonstrates the value of stepwise micro-Raman mapping for the study of phase changes. The results reveal that in unstressed, nominally tetragonal zirconia, there are significant concentrations of the monoclinic phase located at the grain boundaries. The results also confirm that grain boundaries play an important role in the distribution of the monoclinic phase in stressed MgO-stabilized zirconia and that they can act as boundaries to stop transformation. In addition, it has been shown from broadening of the monoclinic phase distribution across the grain boundaries after stress, that they can provide a possible route for stress relief. In some instances phase transformation after indentation was not associated with any visible surface feature. In these instances it is suggested that microcracks are responsible for the pattern of phase transformation.

Acknowledgement

This work has been carried out with the support of Procurement Executive, Ministry of Defence.

References

1. R. C. GARVIE, in "High Temperature Oxides, Part II" (Academic Press, New York, 1970) p. 118.
2. J. D. McCULLOUGH and K. N. TRUEBLOOD, *Acta Crystallogr.* **12** (1959) 507.

3. D. K. SMITH and H. W. NEWKIRK, *ibid.* **18** (1965) 983.
4. G. TEUFER, *ibid.* **15** (1962) 1187.
5. G. M. WOLTEN, *ibid.* **17** (1964) 763.
6. *Idem. J. Amer. Ceram. Soc.* **46** (1963) 418.
7. B. C. WEBER, Aerospace Research Laboratories Report ARL-64-205 (1964).
8. G. KATAGIRI, H. ISHIDA, A. ISHITANI and T. MASAKI, *Adv. Ceram.* **24** (1988) 537.
9. T. ARAHORI, T. SHIGEMATSU and H. YOSHINAGA, *Sumitomo Search* **36** (1988) 97.
10. T. ARAHORI, T. SUZUKI, N. IWAMOTO and N. UMESAKI, *Adv. Ceram.* **24** (1988) 549.
11. D. R. CLARKE and F. ADAR, *J. Amer. Ceram. Soc.* **65** (1982) 284.
12. M. ISHITSUKA, T. SATO, T. ENDO, M. SHIMADA and H. ARASHI, *J. Mater. Sci. Lett.* **8** (1989) 638.
13. R. H. DAUSKARDT, D. K. VEIRS and R. O. RITCHIE, *J. Amer. Ceram. Soc.* **72** (1989) 1124.
14. S. KUDO, J. MIZUNO and H. HASEGAWA, *Adv. Ceram.* **24** (1988) 103.
15. M. BOWDEN, G. D. DICKSON, D. J. GARDINER and D. WOOD, *Appl. Spectrosc.* **44** (1990) 1679.
16. F. J. BERGIN and C. G. SHELTON, in "Proceedings of the IXth International Conference on Raman Spectroscopy", London 1988, edited by R. J. H. Clark and D. A. Long (Wiley, New York, 1988), p. 445.
17. O. OHTAKA and S. KUME, *J. Amer. Ceram. Soc.* **71** (1988) C164.
18. A. ISHITANI, G. KATAGIRI, H. ISHIDA and T. MASAKI, *Microbeam Anal.* (1988) 169.
19. E. D. WHITNEY, *Trans. Faraday Soc.* **61** (1965) 1991.
20. J. ADAMS and B. COX, *J. Nucl. Energy Part A* **11** (1959) 31.
21. R. C. GARVIE and P. S. NICHOLSON, *J. Amer. Ceram. Soc.* **55** (1972) 303.

Received 14 November 1991
and accepted 17 January 1992